Hyperpolarizability and operational magic wavelength in an optical lattice clock

(Article begins on next page)

26 August 2022

Hyperpolarizability and operational magic wavelength in an optical lattice clock

R. C. Brown,[1, *] N. B. Phillips,[1, †] K. Beloy,[1] W. F. McGrew,[1, 2] M. Schioppo,[1, ‡] R. J. Fasano,[1, 2] G. Milani,[1, §] X. Zhang,[1, ¶] N. Hinkley,[1, 2, †] H. Leopardi,[1, 2] T. H. Yoon,[1, **] D. Nicolodi,[1] T. M. Fortier,[1] and A. D. Ludlow[1, ††]

[1] *National Institute of Standards and Technology, 325 Broadway, Boulder, Colorado 80305, USA*[‡‡]
[2] *University of Colorado, Department of Physics, Boulder, Colorado 80309, USA*

(Dated: August 25, 2017)

Optical clocks benefit from tight atomic confinement enabling extended interrogation times as well as Doppler- and recoil-free operation. However, these benefits come at the cost of frequency shifts that, if not properly controlled, may degrade clock accuracy. Numerous theoretical studies have predicted optical lattice clock frequency shifts that scale nonlinearly with trap depth. To experimentally observe and constrain these shifts in an ^{171}Yb optical lattice clock, we construct a lattice enhancement cavity that exaggerates the light shifts. We observe an atomic temperature that is proportional to the optical trap depth, fundamentally altering the scaling of trap-induced light shifts and simplifying their parametrization. We identify an "operational" magic wavelength where frequency shifts are insensitive to changes in trap depth. These measurements and scaling analysis constitute an essential systematic characterization for clock operation at the 10^{-18} level and beyond.

Optical dipole trapping has risen from theory [1] to establish itself as a workhorse experimental technique in numerous contexts [2–5]. Despite the fact that dipole trapping is achieved by inducing large light shifts, it has found prominence in quantum metrology and precision measurements. The concept of magic wavelength trapping resolves this apparent contradiction by inducing large but *identical* shifts on two atomic states of interest [6]. In an optical clock, the energy difference of these two states gives the frequency reference that serves as the timebase. The magic wavelength allows optical lattice clocks [7] to realize the unperturbed atomic transition frequency while maintaining the experimental benefits of trapped systems. Magic wavelength trapping has found applications far beyond atomic clocks including: cavity QED [8], ultracold molecules [9] and Rydberg gases [10], atomic qubits [11, 12], laser cooling [13], and quantum simulation [14, 15].

Magic wavelength optical lattices have enabled optical clocks to achieve unprecedented levels of performance, with fractional frequency instability approaching 1×10^{-18} [16–20] and total systematic uncertainty in the 10^{-18} range [17–19]. Consequently, optical clocks become sensitive tools to measure the gravitational red shift and geopotential [21–24], search for dark matter [25–27], constrain physics beyond the Standard Model [28–30], improve very long baseline interferometry [31], and ultimately redefine the second [32]. However, at these performance levels, the concept of magic wavelength confinement breaks down [33, 34]. Higher-order couplings, including magnetic dipole (M1), electric quadrupole (E2), and hyperpolarizability, prevent a complete cancellation of the light shifts between clock states, introducing shifts that scale nonlinearly with trap depth.

In an ^{171}Yb optical lattice clock, we measure nonlinear light shifts, offering improved determinations of the hyperpolarizability and lattice magic frequency ν_{magic} [35–

38]. Theoretical studies suggest that these higher-order light shifts yield lattice-band-dependent effects [34, 39–41] which vary with atomic temperature, complicating characterization of the light shift and its appropriate extrapolation to zero. In this Letter, we extend the theory and experimentally study these temperature-dependent effects. Doing so reveals a simplification in the shift's functional form, achieving 1.2×10^{-18} clock shift uncertainty. The nonlinear shifts offer an experimental benefit in the form of 'operational magic wavelength' behavior - where the polarizability can be tuned, with laser frequency, to partially compensate the hyperpolarizability and yield linear shift insensitivity to trap depth. These measurements and analysis are relevant for other atomic species, including ^{87}Sr, where the role of hyperpolarizability for accurate characterization of lattice light shifts differs between studies [18, 19, 42–45].

The dominant optical-trap AC Stark effect is from electric dipole polarizability (α_{E1}), giving a shift that scales to leading order with trap depth, U. The differential shift of the clock transition is eliminated by operating at the magic wavelength (or frequency) [33]. Higher multipolarizabilities from magnetic dipole and electric quadrupole contributions (denoted here as α_{M1E2}) also yield shifts, albeit much smaller than the electric dipole terms. The hyperpolarizability (β) shift accounts for electric dipole effects that are fourth order in the electric field. In general the frequency shift on the clock transition, $\delta\nu_{\text{clock}}$, is:

$$\frac{\delta\nu_{\text{clock}}}{\nu_{\text{clock}}} = -U \, \Delta\alpha'_{E1} \, X_{\mathbf{n}} - U \, \Delta\alpha'_{M1E2} \, Y_{\mathbf{n}} - U^2 \, \Delta\beta' \, Z_{\mathbf{n}},$$

(1)

where all quantities appearing on the right-hand-side are dimensionless. Here, Δ denotes a difference in a quantity between clock states, and $\Delta\alpha'_{E1} = \Delta\alpha_{E1} E_r / \alpha_{E1}(\nu_{\text{magic}}) h\nu_{\text{clock}}$, $\Delta\alpha'_{M1E2} = \Delta\alpha_{M1E2} E_r / \alpha_{E1}(\nu_{\text{magic}}) h\nu_{\text{clock}}$, $\Delta\beta' =$
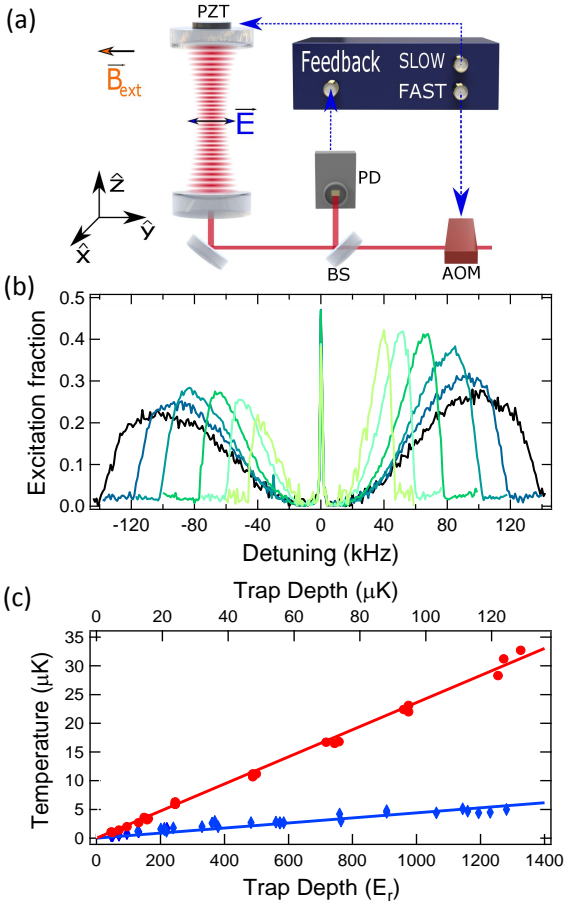
FIG. 1. (a) Schematic of the vertically-oriented lattice build up cavity, with out-of-vacuum mirrors. PD photodiode, BS beamsplitter, AOM acousto-optical modulator, PZT piezo-electric transducer. (b) Sideband spectra for multiple trap depths from 150 E_r (light green trace) to 1260 E_r (black trace). (c) Longitudinal temperatures, extracted from sideband spectra, as a function of trap depth. The red trace corresponds to normal operating conditions, while the blue trace incorporates an additional step of sideband cooling.

$\Delta\beta E_r^2/\alpha_{E1}(\nu_{\text{magic}})^2 h\nu_{\text{clock}}$. $X_\mathbf{n}$, $Y_\mathbf{n}$, and $Z_\mathbf{n}$ represent expectation values of the spatial portion of the trapping potential, $\mathcal{U}(z,\rho) = \exp\left(-2\rho^2/w_0^2\right)\cos^2(kz)$, for motional state $\mathbf{n}$ with $1/e^2$ lattice-beam-intensity radius w_0; $X_\mathbf{n} \equiv \langle\mathbf{n}|\mathcal{U}(z,\rho)|\mathbf{n}\rangle$, $Y_\mathbf{n} \equiv \langle\mathbf{n}|\mathcal{U}(z+\pi/(2k),\rho)|\mathbf{n}\rangle$, $Z_\mathbf{n} \equiv \langle\mathbf{n}|\mathcal{U}(z,\rho)^2|\mathbf{n}\rangle$. U, which is proportional to the lattice intensity, is the dimensionless ratio of trap depth to recoil energy $E_r = \frac{\hbar^2 k^2}{2m}$, where $k = 2\pi\nu_l/c$ for lattice frequency ν_l, $h = 2\pi\hbar$ is Planck's constant, c is the speed of light, and m is the mass of ^{171}Yb.

Here, we extend the perturbative treatment in the harmonic motional-state basis [41] to consider not only longitudinal confinement along the 1-D optical lattice, but also transverse optical confinement. The resulting lattice induced shift for an atom in longitudinal lattice band n_z

and transverse motional state $n_\rho = n_x + n_y$ is:

$$\frac{\delta\nu_{\text{clock}}}{\nu_{\text{clock}}} = n_5\Delta\alpha'_{M1E2}+[(n_1+n_2)\Delta\alpha'_{E1}-n_1\Delta\alpha'_{M1E2}]U^{\frac{1}{2}}$$
$$-[\Delta\alpha'_{E1}+(n_3+n_4+4n_5)\Delta\beta']U+[2\Delta\beta'(n_1+n_2)]U^{\frac{3}{2}}-\Delta\beta'U^2. \tag{2}$$

This treatment yields a $U^{1/2}$ scaling originating from α_{M1E2} [34, 39] and a $U^{3/2}$ scaling originating from β [40] and now includes contributions from both the transverse and longitudinal motional quantum numbers: $n_1 = (n_z+1/2)$, $n_2 = \frac{\sqrt{2}}{kw_0}(n_\rho+1)$, $n_3 = \frac{3}{2}(n_z^2+n_z+1/2)$, $n_4 = \frac{8}{3k^2w_0^2}(n_\rho^2+2n_\rho+3/2)$, and $n_5 = \frac{1}{\sqrt{2}kw_0}(n_z+1/2)(n_\rho+1)$.

Since measurements cannot be made at zero trap depth, extrapolation to the unperturbed clock transition frequency at $U=0$ is required. For shallow traps with cold low-density atomic samples, an extrapolation linear in U has generally been considered sufficient to determine the magic wavelength and unperturbed atomic frequency at the 10^{-17} level of clock uncertainty. However, as the required accuracy increases, the higher order terms in Eq. (2) cannot, in general, be neglected. The added fit parameters from each U-dependent term place a heavy statistical burden on the measurement in order to reach the desired level of uncertainty. Furthermore, the inclusion of these higher-order terms introduces contributions dependent on the thermally averaged $\langle\mathbf{n}\rangle$. In order to meaningfully apply Eq. (2) to experimental data, the $\langle\mathbf{n}\rangle$ must be characterized over the range of U measured.

To experimentally observe light shifts in an ^{171}Yb optical lattice clock [16], we use a power enhancement cavity (finesse ≈ 200 at ν_l, transparent at ν_{clock}) to form the optical lattice, Fig. 1(a). Doing so enables us to realize trap depths greater than $10\times$ our anticipated operational depth. A relatively large lattice beam radius (170 μm) in the transverse plane enables high trapped atom number with relatively low atomic density and thus small density-dependent collisional shifts. The cavity orientation along gravity suppresses resonant tunneling between lattice sites [46, 47]. To ensure that the optical lattice has no significant residual circular polarization (e.g. vacuum window birefringence), the difference frequency between π-transitions from both $m_F = \pm 1/2$ [48] states is measured for all U. Residual circular polarization would lead to a U-dependent vector AC Stark shift in the observed splitting. No such dependence is observed, allowing us to constrain lattice ellipticity below 0.6%. Using the vector AC Stark splitting as an in-situ atomic sensor of optical lattice polarization allows us to exclude polarization-dependent variations in the observed hyperpolarizability effect [36]. The lattice laser frequency is stabilized, over the course of a measurement, to a cavity with a typical drift of $\lesssim 100$ kHz per day. When data were collected, the absolute lattice laser frequency was measured to within ≈ 10 kHz by optically dividing it down to RF [49], via an

octave-spanning Ti:sapphire optical frequency comb [50], and counting it against a calibrated hydrogen maser.

Atomic temperature in both the longitudinal and transverse lattice dimensions, as well as the magnitude of U, is assessed for all clock shift measurements via motional sideband spectroscopy, Fig. 1(b) [51]. We observe that the temperature scales predominantly linear in U, Fig. 1(c). We attribute this linear scaling to the interplay of lattice induced light shifts on the $^1S_0 \rightarrow {}^3P_1$ cooling transition and the atomic kinetic energy cutoff imposed by the finite lattice depth. The linear scaling of temperature with U has important consequences: for our observed ratio of temperature to trap depth, the following lowest-order approximations hold: $\langle n_1 \rangle, \langle n_2 \rangle \propto \sqrt{U}$ and $\langle n_3 \rangle, \langle n_4 \rangle, \langle n_5 \rangle \propto U$. Under these conditions, Eq. (2) can be reduced to:

$$\delta\nu_{\mathrm{clock}}/\nu_{\mathrm{clock}} = -\alpha^* U - \beta^* U^2, \qquad (3)$$

with U-independent finite-temperature polarizabilities α^* and β^* (see Supplemental).

Intensity dependent light shifts were measured with interleaved comparisons of the frequency shift between test- and reference-lattice depth clock configurations, as in Ref. [36]. Sideband spectra were taken directly before or after interleaved clock comparison. The density shift was independently measured as a function of trap depth to apply small ($< 4 \times 10^{-18}$) corrections to the measured light-shift data. The effect of these corrections is small compared to the statistical uncertainty of the deduced magic wavelength. For a given lattice frequency, the clock shifts at multiple trap depths were compared. This frequency shift data is plotted in Fig. 2(a). Each color represents data sets with a distinct ν_l. The uncertainties in $\delta\nu_{\mathrm{clock}}/\nu_{\mathrm{clock}}$ are the total Allan deviation at the end of each data run ($\approx 1 \times 10^{-17}$).

We analyze the experimental data in Fig. 2(a) by fitting each data set to a modified form of Eq. (3) (plus a constant term to account for the $U \neq 0$ reference condition). In principle, a fit with a single quadratic coefficient could be justified because hyperpolarizability has negligible lattice frequency dependence in the vicinity of the magic wavelength. Nevertheless, it is possible for $\Delta\alpha_{E1}$ effects to couple to β^*, giving the quadratic-shift-coefficient dependence on lattice frequency. For example, this situation can arise from atomic temperature that scales nonlinear in the trap depth. Therefore, we perform fits with and without a global β^*, with both methods yielding a mean value of $\beta^* = -5.5(2) \times 10^{-22}$ [52]. The observed coefficient is reduced in magnitude relative to $\Delta\beta'$ by the finite temperature of the system; intuitively atoms in higher motional states are more spatially delocalized and thus experience lower average lattice laser intensity. Nonlinear scaling of the atomic temperature can have other important consequences, such as lattice light shifts with additional U-dependencies that
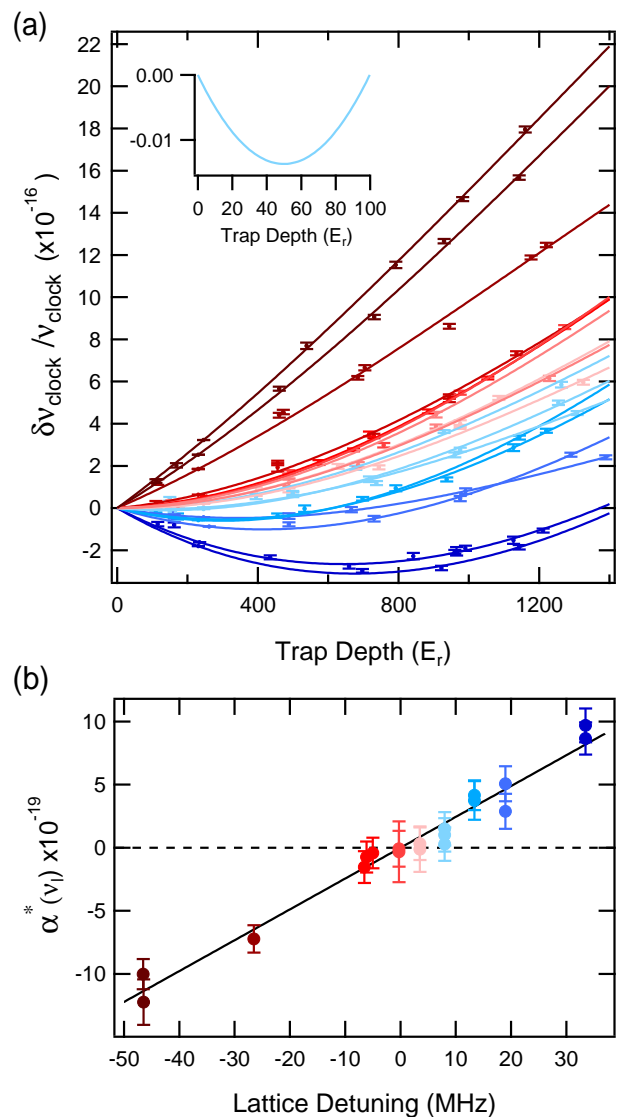

FIG. 2. (a) Clock shifts as a function of lattice depth. Colored traces represent data sets with distinct detunings of ν_l from ν_{zero} from ≈ -50 MHz (dark red) to ≈ 30 MHz (dark blue). This color scheme is quantified in Fig. 2(b). Inset) At the operational magic wavelength for a 50 E_r lattice depth, a 10% change in trap depth creates a 1×10^{-19} change in $\delta\nu_{\mathrm{clock}}/\nu_{\mathrm{clock}}$. (b) Linear coefficients from the global fit, primarily proportional to $\Delta\alpha_{E1}$, as a function of lattice detuning from ν_{zero}. This data is corrected for measured density shifts but not for calculated M1/E2 effects.

must be included in Eq. (3) for high accuracy determination of the shift. Because we have observed a residual quadratic dependence of the atomic temperature in the transverse dimensions versus trap depth, when performing the fit of experimental data, we also allow for a U^3-dependent fit term (see Supplemental). The linear coefficients, α^*, extracted from the fits to data in Fig. 2(a), are shown in Fig. 2(b). These coefficients scale linearly with the lattice detuning and are parameterized as $\alpha^*(\nu_l) =$
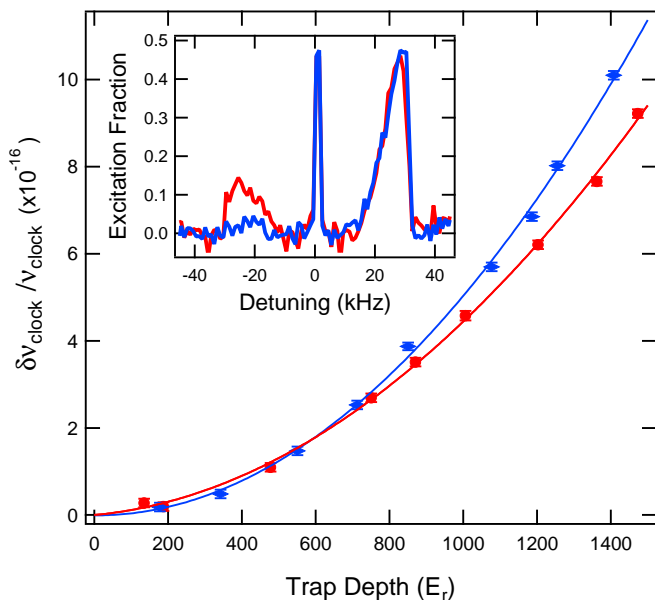
FIG. 3. To experimentally explore the role of finite temperature effects, we measure $\delta\nu_{\mathrm{clock}}/\nu_{\mathrm{clock}}$ near ν_{zero} both with (blue data) and without (red data) sideband cooling. Since the cooler atoms are more localized in the high-intensity portion of the lattice, they experience a larger shift originating from the hyperpolarizability. The inset shows representative sideband traces.

$(\partial\alpha^*/\partial\nu_l) \times (\nu_l - \nu_{\mathrm{zero}})$. Fitting to this functional form, we find $\partial\alpha^*/\partial\nu_l = 2.46(10) \times 10^{-20} \frac{1}{\mathrm{MHz}}$ and that the linear shift vanishes at $\nu_{\mathrm{zero}} = 394,798,267 \pm 1$ MHz. Using a second independent atomic system with similar experimental conditions, we observe consistent values of $\partial\alpha^*/\partial\nu_l$, β^*, and ν_{zero} between the two systems. For anticipated clock operation with a trap depth of 50 E_r, our determinations of α^* and β^* are sufficient to realize 10^{-18} uncertainty.

By inspection of Eq. (2), and recalling that, to leading order, $\langle n_1 \rangle, \langle n_2 \rangle \propto \sqrt{U}$ and $\langle n_5 \rangle \propto U$, we see that both E1 and M1/E2 frequency shifts scale linearly with U. Hence, under these conditions, the dominant effect of M1/E2 contributions is to move the observed zero value of the linear shift away from the lattice frequency where $\Delta\alpha_{E1} = 0$, $\nu_{\mathrm{zero}} = \nu_{\mathrm{magic}} - \nu_{M1E2}$. To estimate the M1/E2 contribution to ν_{zero}, we perform a configuration interaction plus many-body perturbation theory calculation [53] and determine $\alpha'_{M1E2} = 4(4) \times 10^{-8} \left(\frac{E_r}{h\nu_{\mathrm{clock}}}\right)$ corresponding to $\nu_{M1E2} \approx -400$ kHz. This result follows from the partial cancellation of larger terms, yielding a large relative uncertainty. Although ν_{magic} can be deduced from our experimentally measured ν_{zero} and theoretically calculated ν_{M1E2}, it is worth reiterating that ν_{zero} represents an experimentally relevant quantity to zero all linear shifts in Eq. (3).

To highlight the important role of atomic temperature,

we measure the lattice light shifts under two distinct thermal conditions. Figure 3 displays the light shift versus trap depth with and without an additional stage of cooling along the lattice axis dimension, using quenched sideband cooling on the ultra-narrow ${}^1S_0 \to {}^3P_0$ clock transition [37, 54]. The 1-D quenched sideband cooling reduces the longitudinal temperature by a factor of ≥ 6. The blue curve in Fig. 1(c) shows that, after sideband cooling, the longitudinal temperature still exhibits a predominantly linear dependence on trap depth, though its value ranges from just 400 nK to 5 μK. In Fig. 3, the observed shifts are larger in the cooled case, since the near unit fractional population in the ground lattice band experiences the highest lattice laser intensity. In particular, the measured hyperpolarizability effect in the sideband-cooled case increases β^* by 12(5)%. The change in β^* introduced by cooling in just one dimension underscores the importance of characterizing thermal effects on lattice shifts.

Using the preceding expressions and taking into account thermal effects, we translate the measured β^* and α^* to the respective atomic properties $\Delta\beta' \approx -10 \times 10^{-22}$ and $\partial\Delta\alpha'_{E1}/\partial\nu_l \approx 4 \times 10^{-20} \frac{1}{\mathrm{MHz}}$. Alternatively, known lifetime and polarizability data can be used to calculate $\partial\Delta\alpha'_{E1}/\partial\nu_l = 4.5(3) \times 10^{-20} \frac{1}{\mathrm{MHz}}$. While agreement between perturbative theory and experiment is reassuring, the perturbative treatment does not fully account for anharmonic and cross-dimensional effects relevant for higher-lying motional states. We have developed more sophisticated models to evaluate Eq. (1) accounting for these effects [55]. Importantly, we find a key behavior is maintained in more refined analyses: given a linear relationship between temperature and depth, the clock shift is well-approximated by Eq. (3) with α^* and β^* being independent of depth.

The fitted parameters enable us to identify a U-dependent *operational* magic frequency. Neglecting any residual U^3 shift dependence or β^* detuning dependence, $\nu_{\mathrm{opmagic}} \equiv (-2\beta^* U)/(\partial\alpha^*/\partial\nu_l) + \nu_{\mathrm{zero}}$. At this value of ν_l, a negative linear light shift partially cancels the positive hyperpolarizability shift, yielding a shift at the operational U with zero first-order sensitivity to fluctuations in U. Considering several factors (namely: large trap volume for small density shift, low excited-band tunneling rate, and small absolute lattice induced shift), we choose a 50 E_r lattice depth, sufficient for clock operation with 10^{-18} uncertainty. Solving for a minimum at 50 E_r, the measurements in Fig. 2 indicate an operational magic wavelength of 2.2(1) MHz above ν_{zero}. Although typically controlled at the 1% level, a 10% change in trap depth creates a $< 1 \times 10^{-19}$ change in $\delta\nu_{\mathrm{clock}}/\nu_{\mathrm{clock}}$. This parameter regime is shown as an inset in Fig. 2(a).

While the combination of hyperpolarizability and lattice detuning are useful for achieving operational magic wavelengths, they can also obscure determination of ν_{zero} and ν_{clock} when deduced from measurements experimen-

tally limited to a restricted range of U, as is common without a lattice power enhancement cavity. In the simplest case, one can mistake a local minimum for a flat line (over a restricted range of U) leading to extrapolation errors in ν_{clock} and incorrect determinations of ν_{zero}. Consider our measured parameters ($\beta^* = -5.5(2) \times 10^{-22}$, $\partial\alpha^*/\partial\nu_l = 2.46(10) \times 10^{-20} \frac{1}{\text{MHz}}$) and experimental shift uncertainties $\pm 1 \times 10^{-17}$, but now with a maximum trap depth of $300\,E_r$. For a measurement range of 100 to $300\,E_r$, the variation of lattice light shifts would be $< 6 \times 10^{-18}$ at a detuning of 8.9 MHz from ν_{zero} (the operational magic wavelength for the middle of the measurement interval: $200E_r$). At this detuning, the clock shift would appear independent of U, giving the illusion of magic wavelength operation and making it statistically challenging to resolve hyperpolarizability or non-magic linear shifts [56]. Linearly extrapolating to $U = 0$, errors in $\delta\nu_{\text{clock}}/\nu_{\text{clock}}$ of 2×10^{-17} could result. Furthermore, not accounting for hyperpolarizability in the determination of ν_{zero} yields a 8.9 MHz error in the deduced magic wavelength. Such a difficulty in resolving hyperpolarizability and the resulting error in the light shift determination is general for all lattice laser frequencies (not restricted to ν_{opmagic}) and may apply to other atomic species. The case of ^{87}Sr is notable, due to previous measurements and disagreement about the role of hyperpolarizability [18, 19, 42–45]. While the scaling of atomic temperature with trap depth has not been fully considered, experimental parameters have been reported for strontium ($\Delta\beta' = -10(3) \times 10^{-22}$ [44], $\Delta\beta' = -7(7) \times 10^{-22}$ [19], and $\partial\alpha'_{E1}/\partial\nu_l = 3.6(3) \times 10^{-20} \frac{1}{\text{MHz}}$ [58]). A similar analysis to that above finds linear versus non-linear extrapolations over the same limited range of U leads to differences in the shift determination $\delta\nu_{\text{clock}}/\nu_{\text{clock}}$ of $(2-4) \times 10^{-17}$. It seems that the role of non-linear extrapolations in ^{87}Sr will hinge on developing consensus on the magnitude of β^*, including a proper accounting of the temperature scaling with U. Furthermore, this consideration can guide ongoing work in Mg [59], Hg [60], and Cd [61].

In conclusion, we have precisely characterized optical lattice induced light shifts including nonlinear hyperpolarizability effects. Our measurements highlight the importance of finite temperature effects at 10^{-18} fractional frequency accuracy. We have also experimentally demonstrated a metrologically useful regime, the operational magic wavelength, where changes in light shifts can be minimized as the trap depth changes. Furthermore, by implementing quenched sideband cooling along the 1-D lattice axis, tunneling related shifts are suppressed, while somewhat warmer transverse temperatures reduce overall lattice light shifts. These measurements further lay the framework for controlling lattice light shifts at the 10^{-19} level.

---

[*] present address: Georgia Tech Research Institute, Atlanta, GA 30332, USA; brown171@gatech.edu

[†] present address: Stable Laser Systems, Boulder, Colorado, USA

[‡] present address: National Physical Laboratory (NPL), Teddington, TW11 0LW, United Kingdom

[§] permanent address: Istituto Nazionale di Ricerca Metrologica, Strada delle Cacce 91, 10135 Torino, Italy; Politecnico di Torino, Corso duca degli Abruzzi 24, 10125 Torino, Italy

[¶] permanent address: State Key Laboratory of Advanced Optical Communication Systems and Networks, Institute of Quantum Electronics, School of Electronics Engineering and Computer Science, Peking University, Beijing 100871, China

[**] permanent address: Department of Physics, Korea University, 145 Anam-ro, Seongbuk-gu, Seoul 02841, South Korea

[††] andrew.ludlow@nist.gov

[‡‡] Contribution of U.S. government; not subject to copyright.

[1] V. Letokhov, JETP Lett. **7**, 272 (1968).

[2] R. Grimm, M. Weidemüller, and Y. B. Ovchinnikov, Advances in Atomic Molecular and Optical Physics **42**, 95 (2000).

[3] I. Bloch, J. Dalibard, and W. Zwerger, Reviews of Modern Physics **80**, 885 (2008).

[4] H. J. Kimble, Nature **453**, 1023 (2008).

[5] Y. O. Dudin, A. G. Radnaev, R. Zhao, J. Z. Blumoff, T. A. B. Kennedy, and A. Kuzmich, Phys. Rev. Lett. **105**, 260502 (2010), URL http://link.aps.org/doi/10.1103/PhysRevLett.105.260502.

[6] J. Ye, H. Kimble, and H. Katori, Science **320**, 1734 (2008).

[7] M. Takamoto, F.-L. Hong, R. Higashi, and H. Katori, Nature **435**, 321 (2005).

[8] J. McKeever, J. R. Buck, A. D. Boozer, A. Kuzmich, H.-C. Nägerl, D. M. Stamper-Kurn, and H. J. Kimble, Phys. Rev. Lett. **90**, 133602 (2003), URL https://link.aps.org/doi/10.1103/PhysRevLett.90.133602.

[9] J. G. Danzl, M. J. Mark, E. Haller, M. Gustavsson, R. Hart, J. Aldegunde, J. M. Hutson, and H.-C. Nägerl, Nature Physics **6**, 265 (2010).

[10] E. A. Goldschmidt, D. G. Norris, S. B. Koller, R. Wyllie, R. C. Brown, J. V. Porto, U. I. Safronova, and M. S. Safronova, Phys. Rev. A **91**, 032518 (2015), URL http://link.aps.org/doi/10.1103/PhysRevA.91.032518.

[11] N. Lundblad, M. Schlosser, and J. V. Porto, Phys. Rev. A **81**, 031611 (2010), URL http://link.aps.org/doi/10.1103/PhysRevA.81.031611.

[12] J. Yang, X. He, R. Guo, P. Xu, K. Wang, C. Sheng, M. Liu, J. Wang, A. Derevianko, and M. Zhan, Phys. Rev. Lett. **117**, 123201 (2016), URL https://link.aps.org/doi/10.1103/PhysRevLett.117.123201.

[13] P. M. Duarte, R. A. Hart, J. M. Hitchcock, T. A. Corcovilos, T.-L. Yang, A. Reed, and R. G. Hulet, Phys. Rev. A **84**, 061406 (2011), URL http://link.aps.org/doi/10.1103/PhysRevA.84.061406.

[14] F. Scazza, C. Hofrichter, M. Höfer, P. De Groot, I. Bloch, and S. Fölling, Nature Physics **10**, 779 (2014).

[15] G. Cappellini, M. Mancini, G. Pagano, P. Lombardi, L. Livi, M. S. De Cumis, P. Cancio, M. Pizzocaro, D. Calonico, F. Levi, et al., Physical review letters **113**, 120402 (2014).

[16] N. Hinkley, J. A. Sherman, N. B. Phillips, M. Schioppo, N. D. Lemke, K. Beloy, M. Pizzocaro, C. W. Oates, and A. D. Ludlow, Science **341**, 1215 (2013), URL http://www.sciencemag.org/content/341/6151/1215.abstract.

[17] B. Bloom, T. Nicholson, J. Williams, S. Campbell, M. Bishof, X. Zhang, W. Zhang, S. Bromley, and J. Ye, Nature **506**, 71 (2014).

[18] I. Ushijima, M. Takamoto, M. Das, T. Ohkubo, and H. Katori, Nature Photonics **9**, 185 (2015).

[19] T. Nicholson, S. Campbell, R. Hutson, G. Marti, B. Bloom, R. McNally, W. Zhang, M. Barrett, M. Safronova, G. Strouse, et al., Nature communications **6** (2015).

[20] M. Schioppo, R. C. Brown, W. F. McGrew, N. Hinkley, R. J. Fasano, K. Beloy, T. H. Yoon, G. Milani, D. Nicolodi, J. A. Sherman, et al., Nature Photonics **11**, 48 (2017), URL http://dx.doi.org/10.1038/nphoton.2016.231.

[21] N. Ashby, P. L. Bender, J. L. Hall, J. Ye, S. A. Diddams, S. R. Jefferts, N. Newbury, C. Oates, R. Dolesi, S. Vitale, et al., Proceedings of the International Astronomical Union **5**, 414 (2009).

[22] S. Schiller, G. Tino, P. Gill, C. Salomon, U. Sterr, E. Peik, A. Nevsky, A. Görlitz, D. Svehla, G. Ferrari, et al., Experimental astronomy **23**, 573 (2009).

[23] C.-W. Chou, D. Hume, T. Rosenband, and D. Wineland, Science **329**, 1630 (2010).

[24] T. Takano, M. Takamoto, I. Ushijima, N. Ohmae, T. Akatsuka, A. Yamaguchi, Y. Kuroishi, H. Munekane, B. Miyahara, and H. Katori, Nature Photonics **10**, 662 (2016).

[25] A. Derevianko and M. Pospelov, Nature Physics **10**, 933 (2014).

[26] A. Arvanitaki, J. Huang, and K. Van Tilburg, Physical Review D **91**, 015015 (2015).

[27] P. Wcisło, P. Morzyński, M. Bober, A. Cygan, D. Lisak, R. Ciuryło, and M. Zawada, Nature Astronomy **1**, 0009 (2016).

[28] N. Huntemann, B. Lipphardt, C. Tamm, V. Gerginov, S. Weyers, and E. Peik, Phys. Rev. Lett. **113**, 210802 (2014), URL http://link.aps.org/doi/10.1103/PhysRevLett.113.210802.

[29] C. Delaunay and Y. Soreq, ArXiv e-prints (2016), 1602.04838.

[30] C. Frugiuele, E. Fuchs, G. Perez, and M. Schlaffer, ArXiv e-prints (2016), 1602.04822.

[31] D. Normile and D. Clery, Science **333**, 1820 (2011), ISSN 0036-8075, http://science.sciencemag.org/content/333/6051/1820.full.pdf, URL http://science.sciencemag.org/content/333/6051/1820.

[32] F. Riehle, Comptes Rendus Physique **16**, 506 (2015).

[33] H. Katori, M. Takamoto, V. G. Pal'chikov, and V. D. Ovsiannikov, Phys. Rev. Lett. **91**, 173005 (2003), URL http://link.aps.org/doi/10.1103/PhysRevLett.91.173005.

[34] A. V. Taichenachev, V. I. Yudin, V. D. Ovsiannikov, V. G. Pal'chikov, and C. W. Oates, Phys. Rev. Lett. **101**, 193601 (2008), URL http://link.aps.org/doi/10.1103/PhysRevLett.101.193601.

[35] Z. W. Barber, J. E. Stalnaker, N. D. Lemke, N. Poli, C. W. Oates, T. M. Fortier, S. A. Diddams, L. Hollberg, C. W. Hoyt, A. V. Taichenachev, et al., Phys. Rev. Lett. **100**, 103002 (2008), URL http://link.aps.org/doi/10.1103/PhysRevLett.100.103002.

[36] N. D. Lemke, A. D. Ludlow, Z. W. Barber, T. M. Fortier, S. A. Diddams, Y. Jiang, S. R. Jefferts, T. P. Heavner, T. E. Parker, and C. W. Oates, Phys. Rev. Lett. **103**, 063001 (2009), URL http://link.aps.org/doi/10.1103/PhysRevLett.103.063001.

[37] N. Nemitz, T. Ohkubo, M. Takamoto, I. Ushijima, M. Das, N. Ohmae, and H. Katori, Nature Photonics **10**, 258 (2016).

[38] M. Pizzocaro, P. Thoumany, B. Rauf, F. Bregolin, G. Milani, C. Clivati, G. A. Costanzo, F. Levi, and D. Calonico, Metrologia **54**, 102 (2017), URL http://stacks.iop.org/0026-1394/54/i=1/a=102.

[39] H. Katori, K. Hashiguchi, E. Y. Il'inova, and V. D. Ovsiannikov, Phys. Rev. Lett. **103**, 153004 (2009), URL http://link.aps.org/doi/10.1103/PhysRevLett.103.153004.

[40] V. D. Ovsiannikov, V. G. Pal'chikov, A. V. Taichenachev, V. I. Yudin, and H. Katori, Phys. Rev. A **88**, 013405 (2013), URL http://link.aps.org/doi/10.1103/PhysRevA.88.013405.

[41] H. Katori, V. D. Ovsiannikov, S. I. Marmo, and V. G. Palchikov, Phys. Rev. A **91**, 052503 (2015), URL http://link.aps.org/doi/10.1103/PhysRevA.91.052503.

[42] A. Brusch, R. Le Targat, X. Baillard, M. Fouché, and P. Lemonde, Phys. Rev. Lett. **96**, 103003 (2006), URL http://link.aps.org/doi/10.1103/PhysRevLett.96.103003.

[43] P. G. Westergaard, J. Lodewyck, L. Lorini, A. Lecallier, E. A. Burt, M. Zawada, J. Millo, and P. Lemonde, Phys. Rev. Lett. **106**, 210801 (2011), URL http://link.aps.org/doi/10.1103/PhysRevLett.106.210801.

[44] R. Le Targat, L. Lorini, Y. Le Coq, M. Zawada, J. Guéna, M. Abgrall, M. Gurov, P. Rosenbusch, D. Rovera, B. Nagórny, et al., Nature communications **4** (2013).

[45] S. Falke, N. Lemke, C. Grebing, B. Lipphardt, S. Weyers, V. Gerginov, N. Huntemann, C. Hagemann, A. Al-Masoudi, S. Häfner, et al., New Journal of Physics **16**, 073023 (2014).

[46] The lattice is ≈ 1.5° off of vertical to avoid spurious reflections from view ports.

[47] P. Lemonde and P. Wolf, Phys. Rev. A **72**, 033409 (2005), URL http://link.aps.org/doi/10.1103/PhysRevA.72.033409.

[48] Since ^{171}Yb has a nuclear spin of $I = 1/2$, there is no tensor shift.

[49] T. M. Fortier, M. S. Kirchner, F. Quinlan, J. Taylor, J. Bergquist, T. Rosenband, N. Lemke, A. Ludlow, Y. Jiang, C. Oates, et al., Nature Photonics **5**, 425 (2011).

[50] T. M. Fortier, A. Bartels, and S. A. Diddams, Optics Letters **31**, 1011 (2006).

[51] S. Blatt, J. W. Thomsen, G. K. Campbell, A. D. Ludlow,

M. D. Swallows, M. J. Martin, M. M. Boyd, and J. Ye, Phys. Rev. A **80**, 052703 (2009), URL `http://link.aps.org/doi/10.1103/PhysRevA.80.052703`.

[52] For nonlinear fits with $\chi^2 > 1$, not all fitting routines by default return the same standard errors. In the case of $\chi^2 > 1$, we report uncertainty multiplied by the square root of the reduced χ^2.

[53] V. A. Dzuba and A. Derevianko, Journal of Physics B: Atomic, Molecular and Optical Physics **43**, 074011 (2010), URL `http://stacks.iop.org/0953-4075/43/i=7/a=074011`.

[54] E. A. Curtis, C. W. Oates, and L. Hollberg, Phys. Rev. A **64**, 031403 (2001), URL `http://link.aps.org/doi/10.1103/PhysRevA.64.031403`.

[55] K. Beloy et al., *In preparation.*

[56] According to our simulations, A F-test for higher order terms, at the 5% level with 10, 10^{-17} measurements, would favor the null hypothesis of a lower order fit.

[57] The atomic temperature dependence of hyperpolarizability may not been fully considered in these cases.

[58] C. Shi, J.-L. Robyr, U. Eismann, M. Zawada, L. Lorini, R. Le Targat, and J. Lodewyck, Phys. Rev. A **92**, 012516 (2015), URL `http://link.aps.org/doi/10.1103/PhysRevA.92.012516`.

[59] A. P. Kulosa, D. Fim, K. H. Zipfel, S. Rühmann, S. Sauer, N. Jha, K. Gibble, W. Ertmer, E. M. Rasel, M. S. Safronova, et al., Phys. Rev. Lett. **115**, 240801 (2015), URL `https://link.aps.org/doi/10.1103/PhysRevLett.115.240801`.

[60] R. Tyumenev, M. Favier, S. Bilicki, E. Bookjans, R. L. Targat, J. Lodewyck, D. Nicolodi, Y. L. Coq, M. Abgrall, J. Guna, et al., New Journal of Physics **18**, 113002 (2016), URL `http://stacks.iop.org/1367-2630/18/i=11/a=113002`.

[61] Y. Kaneda, J. M. Yarborough, Y. Merzlyak, A. Yamaguchi, K. Hayashida, N. Ohmae, and H. Katori, Opt. Lett. **41**, 705 (2016), URL `http://ol.osa.org/abstract.cfm?URI=ol-41-4-705`.